Bioactive Materials 5 (2020) 253–259

Contents lists available at ScienceDirect

Bioactive Materials

journal homepage: http://www.keaipublishing.com/biomat

Antibacterial and angiogenic chitosan microneedle array patch for promoting wound healing

Junjie Chi[a,b,c], Xiaoxuan Zhang[a,c], Canwen Chen[a], Changmin Shao[c], Yuanjin Zhao[a,c,*], Yongan Wang[b,**]

[a] Department of Clinical Laboratory, The Affiliated Drum Tower Hospital of Nanjing University Medical School, Nanjing, 210008, China
[b] State Key Laboratory of Toxicology and Medical Countermeasures, Institute of Pharmacology and Toxicology, Academy of Military Medical Sciences, Beijing, 100850, China
[c] State Key Laboratory of Bioelectronics, School of Biological Science and Medical Engineering, Southeast University, Nanjing, 210096, China

ARTICLE INFO

Keywords:
Microneedle
Chitosan
Drug delivery
Wound healing
Patch

ABSTRACT

A patch with the capability of avoiding wound infection and promoting tissue remolding is of great value for wound healing. In this paper, we develop a biomass chitosan microneedle array (CSMNA) patch integrated with smart responsive drug delivery for promoting wound healing. Chitosan possesses many outstanding features such as the natural antibacterial property and has been widely utilized for wound healing. Besides, the microstructure of microneedles enables the effective delivery of loaded drugs into the target area and avoids the excessive adhesion between the skin and the patch. Also, vascular endothelial growth factor (VEGF) is encapsulated in the micropores of CSMNA by temperature sensitive hydrogel. Therefore, the smart release of the drugs can be controllably realized via the temperature rising induced by the inflammation response at the site of wounds. It is demonstrated that the biomass CSMNA patch can promote inflammatory inhibition, collagen deposition, angiogenesis, and tissue regeneration during the wound closure. Thus, this versatile CSMNA patch is potentially valuable for wound healing in clinical applications.

1. Introduction

Skin is one of the most important defensive lines to protect human body from the external microbial invasion and maintain body fluid, electrolytes and nutritional components [1]. Once damaged, the skin would lose its functions and seriously endanger people's physical and mental health [2,3]. Thus, wound healing has invariably been of fundamental research focus in the whole medical field, which leads to severe challenges and serious economic burdens [4,5]. To resolve this problem, patches that can dramatically inhibit bacterial infection and accelerate wound healing are considered as the most efficient and effective medical treatment method. Particularly, with the loading of active drugs, such as bactericidal drugs, hemostatic drugs, anti-inflammatory drugs and angiogenic factors, the patches can realize antibacteria, hemostasis, anti-inflammation and tissue regeneration [6–8]. Moreover, the patches are further developed to integrate with various kinds of microstructures like particles, which endows them with multiple functions and effective drug delivery strategies [9–16]. Thus, by combining the drug delivery system and microstructure, the functional patches have made increasing achievements in wound healing. However, most of the existing patches adopt natural and synthetic polymers, which always require complex biological extraction technique and complicated chemical synthesis procedures [17–21]. Such extraction and synthesis often involve the use of organic reagents and extreme experimental conditions, leading to the reduction of activity and biocompatibility of the active components. In addition, typical patches only possess plain microstructures and dull drug delivery features, restricting their repair effects and further medical applications. Therefore, the development of versatile patches integrated with available polymers and excellent microstructure for controllable drug delivery is significantly anticipated.

In this research, we propose a biomass chitosan hydrogel microneedle array patch with controllable drug release for promoting wound healing, schemed in Scheme 1. Chitosan (CS), a derivative from chitin of arthropod, is the unique alkaline polysaccharide in nature attributed to its positively charged amino group. The extraction process of CS is

Peer review under responsibility of KeAi Communications Co., Ltd.
* Corresponding author. Department of Clinical Laboratory, The Affiliated Drum Tower Hospital of Nanjing University Medical School, Nanjing, 210008, China.
** Corresponding author.
E-mail addresses: yjzhao@seu.edu.cn (Y. Zhao), yonganw@126.com (Y. Wang).

https://doi.org/10.1016/j.bioactmat.2020.02.004
Received 10 December 2019; Received in revised form 2 February 2020; Accepted 3 February 2020

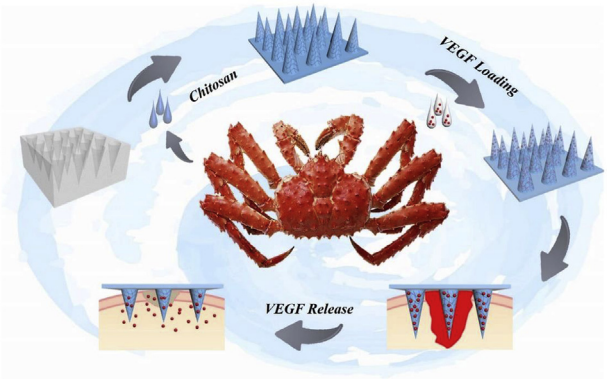

Scheme 1. Scheme of the fabrication and controllable drug release application of the biomass microneedle patch.

also easy-operated, nontoxic, mild and friendly. These features make CS dramatically valuable in biomedical applications with the characteristics of biodegradation, nontoxicity, biocompatibility, antimicrobial and hemostasis [22–26]. Besides, microneedles (MN) could have uniform nano or microstructures by using various kinds of natural materials and synthetic polymers, and could easily penetrate the skin in a minimally invasive manner to effectively deliver drugs to the target areas and maintain local drug concentration in a long term. Benefitting from these advantages, MN has proved its worth in many medical fields including cancer therapy, biomedical sensors and sample collection [27–30]. Therefore, it is conceived that the combination of CS and MN would be conductive to develop a novel patch with the function of smart drug delivery for promoting wound healing.

Herein, we integrated the antibacterial CS hydrogel with the MN array to fabricate a versatile type of patch for promoting wound healing, which could directly and controllably deliver drugs to the damaged areas. The CS hydrogel not only endowed our patch with porous structures, but also gave it antibacterial activity and hemostatic activity. In addition, the microstructure of MN could deliver the loaded drugs into the target area effectively and avoid the excessive adhesion between the skin and the patch. Importantly, active pharmaceutical molecules, vascular endothelial growth factor (VEGF), were encapsulated into the micropores of the chitosan microneedle array (CSMNA) mildly by another smart hydrogel, the temperature responsive poly(N-isopropylacrylamide) (pNIPAM) [31–33]. Actually, the loaded drugs releasing from the CSMNA could be induced through the rise of the body surface temperature attributing to the inflammation response at the site of wounds. It was demonstrated that the CSMNA patch could accelerate the migration and distribution of cells and permit the nutrients and oxygen transportation efficiently, as well as the expelling of metabolic wastes. These features indicate that the versatile CSMNA patch is a superior drug carrier and has tremendous potential for promoting wound healing.

2. Experimental section

Materials and Animals: Chitosan (average Mw 180 kDa), N-isopropylacrylamide (NIPAM), fluorescein isothiocyanate labelled bovine serum albumin (FITC-BSA), NaOH, Vascular endothelial growth factor (VEGF) and 2-hydroxy-2-methylpropiophenone (HMPP) were all obtained from Sigma-Aldrich and used without any treatment. The male Sprague-Dawley rats (8–12-week-old) were provided by Jinling Hospital (Nanjing, China). All rats were treated strictly according to the Laboratory Animal Care and Use Guidelines. All the animal care and experimental procedures were reviewed and approved by the Animal Investigation Ethics Committee of Jinling Hospital.

Characterization: The optical and fluorescence images of CSMN were captured using a microscopy (Olympus SZX16) equipped with a CCD (Olympus DP30BW). SEM images were taken by a scanning electron microscope (SEM, Hitachi S–3000 N). The fluorescence intensity was measured by a fluorescence microscope (Olympus, CKX41) equipped with optic spectrometer. Fluorescence images of LIVE/DEAD bacterial staining were obtained by a laser scanning confocal microscope (Carl Zeiss, LSM510).

Fabrication of the CSMN: The microneedle fabrication was carried out using silicone mold. Chitosan powder was predissolved in a solution of 2% acetic acid by ultrasonic treatment to obtain CS pre-gel. The CS pre-gel was completely infilled into the conical microcavities of the mold under vacuum for 5 min. The excess pre-gel out of the microcavities was removed. Then, the whole mold was immersed into NaOH (10% w/v) aqueous solution to solidify the CS gel. After solidification, wash the mold with deionized water to obtain the CSMN. For drug loading, NIPAM pre-gel solution with different concentrations mixed with VEGF and 1% HMPP was then deposited onto the mold surface followed by vacuum for 30 min to allow the pre-gel solution to infiltrate into the voids of the CSMN. After discarding the excess pre-gel, the mold was irradiated by UV light (365 nm, 100 W) for 1 min under a lower temperature to solidify the NIPAM gel. Finally, CS aqueous solution was cast into the mold and dried under vacuum to form a base for the mechanical support. The resulting CSMN was carefully separated from the mold.

Controllable Drug Release: The controlled release experiment was carried out using FITC-BSA as a demo. FITC-BSA with the concentration of 1 mg/mL was mixed with NIPAM pre-gel and encapsulated into the CSMN by UV polymerization. The CSMN was kept in release buffer of PBS and equilibrated at 40 °C for 5 min to realize a shrinking state. Then it was kept at room temperature (25 °C) for 15 min to recover to the original state. This temperature cycle was taken several times and fluorescence images of the CSMN was captured after every cycle of cooling.

Antibacterial Test in vitro: Gram-positive *Staphylococcus aureus* and Gram-negative *Escherichia coli* were chosen to verify the antibacterial activity of CSMN. Two kinds of bacterial were cultured until the turbidity of the bacterial suspension was around 0.5 based on McFarland standards. Subsequently, the bacterial was collected and resuspended using PBS buffer. The resuspended bacteria were incubated with CSMN respectively in 24-well plates. After 24 h, the suspensions were stained by live-dead dyes and the fluorescence images were captured by confocal microscopy.

Wound Healing Study: A severe infected wound model was used to evaluate the effect of CSMN in wound healing. After being anesthetized, a circular skin at 1 cm in diameter on the back of rats was removed to create a wound. After that 100 μL of bacterial suspension was injected onto the wound area. Then, the rats were divided into four groups and treated with VEGF loaded CSMN, CSMN, plane CS film and PBS solution, respectively. Finally, the rats were put back into separated cages with sufficient water and food. The wounds were observed and photographed on day 0,3,5,7 and 9. After nine days, the rats were sacrificed and regenerated tissues at the wound sites were excised. Each tissue sample was cut into two pieces. One was immersed in 10% neutral formaldehyde for further immunohistochemistry and histology analysis, another was stored in liquid nitrogen for immunofluorescence staining.

Histology, Immunohistochemistry and Immunofluorescence Staining: The samples were embedded in paraffin after dehydration. Serial sections, 5 μm in thickness, were obtained by using a microtome. The sections were used for H&E staining, Masson's trichrome staining, and immunohistochemical analysis. IL-6 and TNF-α staining were used for immunohistochemistry. Primary antibodies CD31 (KEYGEN, KGYM0118-7) and α-smooth muscle actin (KEYGEN, KGYT5053-6) were utilized for neovascularization analysis.

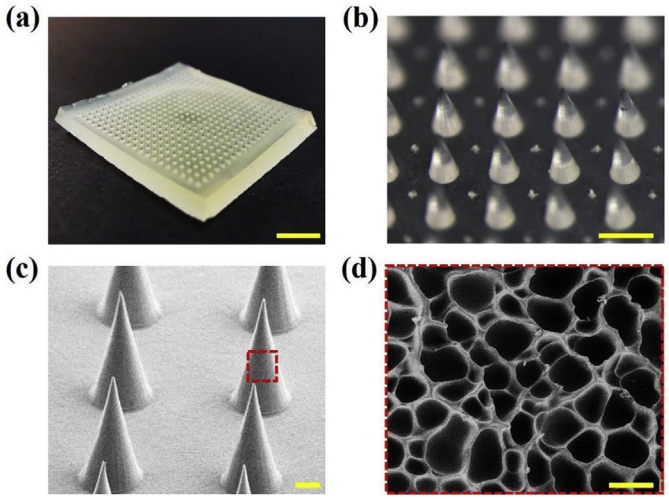

Fig. 1. Optical and SEM images of CSMNA: (a) optical image of CSMNA; (b) micrograph of CSMNA; (c) SEM image of CSMNA; (d) surface microstructure of the CSMNA. Scare bars are 5 mm in (a), 500 μm in (b), 100 μm in (c) and 1 μm in (d).

3. Results and discussion

In a typical experiment, a micromolding approach was used to fabricate the CSMNA array. Briefly, a predetermined amount of CS pre-gel solution was loaded into the microcavities of the mold and kept in the mold under vacuum for 30 min. After that, the mold filled with CS in the microcavities was immersed into sodium hydroxide solution to solidify the CS microneedles. Another round of second pre-gel solution containing active drugs was loaded into the mold and kept under vacuum for 30 min to allow the pre-gel solution to infiltrate into the voids of the CSMNA, which was then solidified by UV light. Finally, CS aqueous solution was cast into the mold and dried under vacuum to form a base for the mechanical support. The resulting CSMNA patch was arranged in a 20 × 20 MN array (Fig. 1a), and each microneedle possessed a conical shape with a tip diameter of 5 μm, a height of 600 μm and a base diameter of 300 μm (Fig. 1b and c). The magnified microstructure of such microneedle was further observed by SEM (Fig. 1d). It was found that the CS microneedle which was not filled with second pre-gel solution presented a porous structure. This feature permitted other solutions like second pre-gel to permeate into the voids by capillary force for drug loading.

It is worth noting that the concentration of the CS crucially determines the size of the pores in the microneedle, which will decide the amount of the loaded drug. In this work, we fabricated CSMNA by using CS with different concentration of 1%, 2%, 3%, 4% and 5%, respectively. The size of the pores was found to decrease when the concentration of CS increased from 2% to 4% (Fig. S1, Supporting Information). Considering that the densely porous microstructure would impede the second pre-gel infiltration and drug content, it could be concluded that the CSMNA with bigger pore size fabricated by low concentration of CS would load more drugs. Besides, it was also found that CS with concentration of 5% was unsuited for fabricating of microneedles because of its poor fluidity, which disallowed the solution to be squeezed into the mold even under vacuum (Figs. S2a–e, Supporting Information). While, a CS solution with the concentration of 1% could not form microneedles effectively owing to the lower mechanical strength resulted from the low content of CS (Fig. S2f, Supporting Information). Therefore, by considering the pore size, the fluidity as well as the hardness together, an optimized CS concentration of 4% was chosen to fabricate CSMNA patch in the following experiments.

Developing patches which could controllably deliver drugs based on stimulation responsive hydrogels is extremely urgent for wound healing, as the one-time release of all loaded drugs cannot assure a long-time repair effect. Here, we utilized pNIPAM hydrogel as a smart temperature-responsive system to controllably release drugs from the CSMNA. For this purpose, drugs were pre-dissolved in the NIPAM precursor solution and then filled into the pores of CSMNA for second polymerization. To investigate the ability of the smart drug delivery system, fluorescein isothiocyanate labelled bovine serum albumin (FITC-BSA) was utilized as a demo to simulate the release of macromolecular drugs from the CSMNA. Then the second polymerized CSMNAs containing FITC-BSA were exposed to the temperature cycle of 40 °C for 5 min and 25 °C for 15 min several times, and the drug release was observed. Notably, when the applied temperature exceeded the volume phase transition temperature (VPTT) of pNIPAM hydrogel, which is typically 37 °C, the pNIPAM hydrogel in the pores of the CSMNAs shrank and the encapsulated FITC-BSA was thus extruded from them to realize the release of drugs. This temperature responsive FITC-BSA release was demonstrated by the gradually decreasing fluorescence intensity of the CSMNA when they were exposed to several times of temperature cycle, as shown in Fig. 2.

Besides, by changing the pNIPAM concentration, the release modes of the CSMNA could be flexibly tuned. It was observed that almost 70% of the BSA was released from the CSMNA by only taking one cycle of temperature exchange with the 5% pNIPAM hydrogel, while five cycles were needed to release almost half of the BSA with the pNIPAM concentration of 20%. In addition, when the hydrogel concentration came up to 25%, the release of BSA did not exceed 20% even after five cycles (Fig. S3, Supporting Information). These different release modes of the

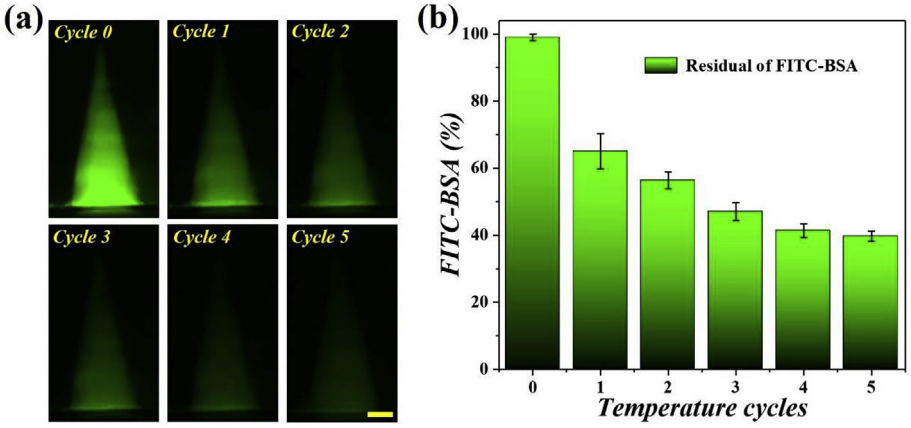

Fig. 2. Temperature responsive drug release simulated by FITC-BSA encapsulated by 15% pNIPAM: (a) fluorescence images of FITC-BSA loaded CSMNA exposed to different temperature cycles; (b) residual of the FITC-BSA under different temperature cycles. Scare bar is 100 μm.

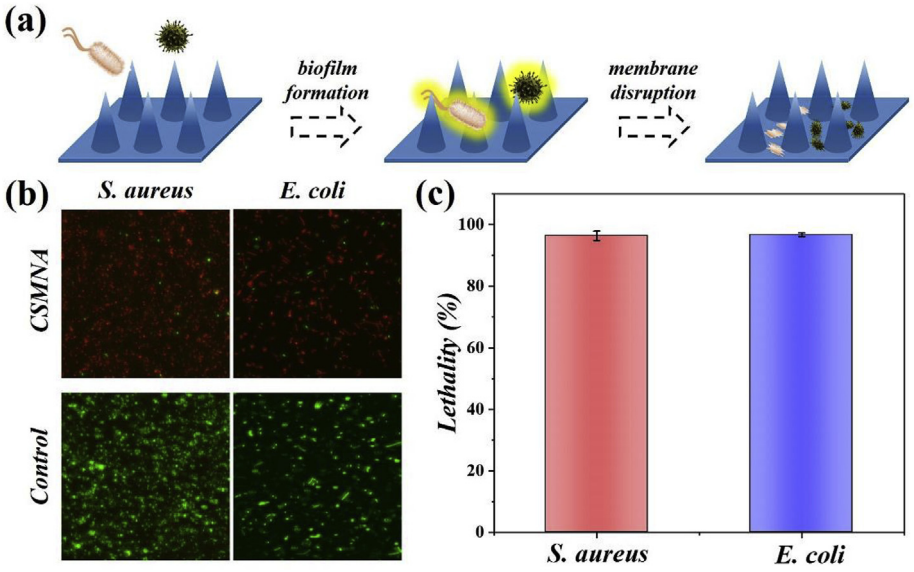

Fig. 3. Antibacterial property of the CSMNA: (a) schematic illustration of anti-infective activity; (b) viability assay of *S. aureus* and *E. coli* co-cultured with the CSMNA and PBS solution, respectively; (c) death rate of *S. aureus* and *E. coli* co-cultured with the CSMNA.

CSMNA with different pNIPAM concentrations were due to the concentration determined intermolecular hydrogen bonds strength. Specifically, a higher concentration of pNIPAM would result in a stronger mechanical strength of the hydrogel which was less affected by temperature change, so that the drug release was slower. This concentration determined trigging condition for drug release would provide versatile choices for smart delivery systems to satisfy various clinical needs.

Besides the porous feature for drug delivery, CS also has inherent antibacterial activity, analgesic effect, hemostatic activity and many other advantages for developing hydrogel wound patches. Thanks to its positively charged property, CS can react with anionic groups on the cell wall or cytomembrane of bacteria via its abundant protonated amino groups and form a biofilm surrounding the bacteria, thus altering the cytomembrane permeability, preventing the intake of nutriments, finally leading to the bacteria lysis (Fig. 3a). To evaluate the antibacterial activity of the CS constituent, the CSMNA with the concentration of 4% was used to culture gram-positive *Staphylococcus aureus* and gram-negative *Escherichia coli*, respectively. The bacterial staining results indicated that both of the bacteria were alive and maintained their inherent shapes in the PBS control group. On the contrary, when co-cultured with the CSMNA, most of the bacteria died, showing that the CSMNA could break the cytomembrane and give rise to the outflow and accumulation of nucleic acid (Fig. 3b). Statistical results also showed that almost 99% of both *S. aureus* and *E. coli* co-cultured with the CSMNA were dead (Fig. 3c). The excellent antibacterial activity of the CS hydrogel endowed the CSMNA patch competitive potentiality for avoiding bacterial infection related complications and promoting wound healing.

To demonstrate the excellent repair capability of the CSMNA patch in promoting wound healing, VEGF encapsulated CSMNA was used for *in vivo* experiments (Fig. 4a). Meanwhile, the CSMNA patch filled with pNIPAM hydrogel only, plane CS film with the same concentration, and PBS group as control were also performed. All the rats were modeled an infectious wound on the back and randomly divided into the above four groups. The wound healing processes in these groups were all recorded by photographs on days 0, 3, 5, 7 and 9 for a detailed analysis (Fig. 4b). These photographs clearly showed that the wound closure rate was higher in the CSMNA patch-treated rats group than that in the control group and plane CS film group. Particularly, with the benefit of VEGF, the wound healing efficiency was dramatically enhanced (Fig. S4a, Supporting Information). Additionally, the hematoxylin and eosin (H&E) staining results presented the regenerated granulation tissue at the wound bed (Fig. 4c). The thickness of the granulation tissue in experimental group of CSMNA with VEGF was 1.80 ± 0.23 mm, which was the maximum. And the minimal thickness was 0.58 ± 0.21 mm in the control group of PBS solution. The granulation tissue in the CSMNA group and plane CS film group were also superior than the control group, which were 1.35 ± 0.25 and 1.10 ± 0.23 mm, respectively (Fig. S4b, Supporting Information).

Thanks to the antibacterial capability as well as the remarkable protective effect of the CS hydrogel, the plane CS film could work as a barrier to prevent the wound suffering from further damage and infection in wound repair and skin regeneration. Thus, the wound healing processes in the plane CS film group were better than that in control group. But, owing to the close contact of wounds and the plane surface of CS films, the air interchange near the regenerating tissue was rather poor, limiting the performance of CS films. By comparison, benefiting from the microneedle structure, the CSMNA patch could not only act as a bactericidal barrier, but also facilitate the air flow between the external environment and regenerating tissue through the microstructure. Therefore, the wound healing process in the group of CSMNA patch filled with pNIPAM hydrogel were mildly better than the plane CS film group. It is worth noting that, with the loading of VEGF by pNIPAM, the CSMNA patch exhibited further better wound-healing effects in the wound closure. After the VEGF encapsulated CSMNA was applied to the wounded sites, the inflammatory reaction gave rise to local skin temperature increase, which induced the pNIPAM hydrogel to shrink in the cores of the CSMNA to promote VEGF release into the wound sites, bringing about the best level of tissue regeneration. These results indicated that the CSMNA patch could provide a versatile smart drug delivery system to maximize the effect of VEGF in promoting wound healing.

During the wound healing process, inflammation is a crucial index that can reflect the infection level and the early stage of the healing condition. Thus, we first analyzed the expression quantity of two typical proinflammatory factors, interleukin-6 (IL-6) and tumor necrosis factor-α (TNF-α), by immunohistochemistry at day 9 (Fig. 5a and b). A mass of IL-6 and TNF-α were obviously observed in the control group, indicating a serious inflammatory response in the wound site. In contrast, IL-6 and TNF-α were all downregulated in the plane CS film, CSMNA patch and CSMNA patch with VEGF encapsulated groups, because the

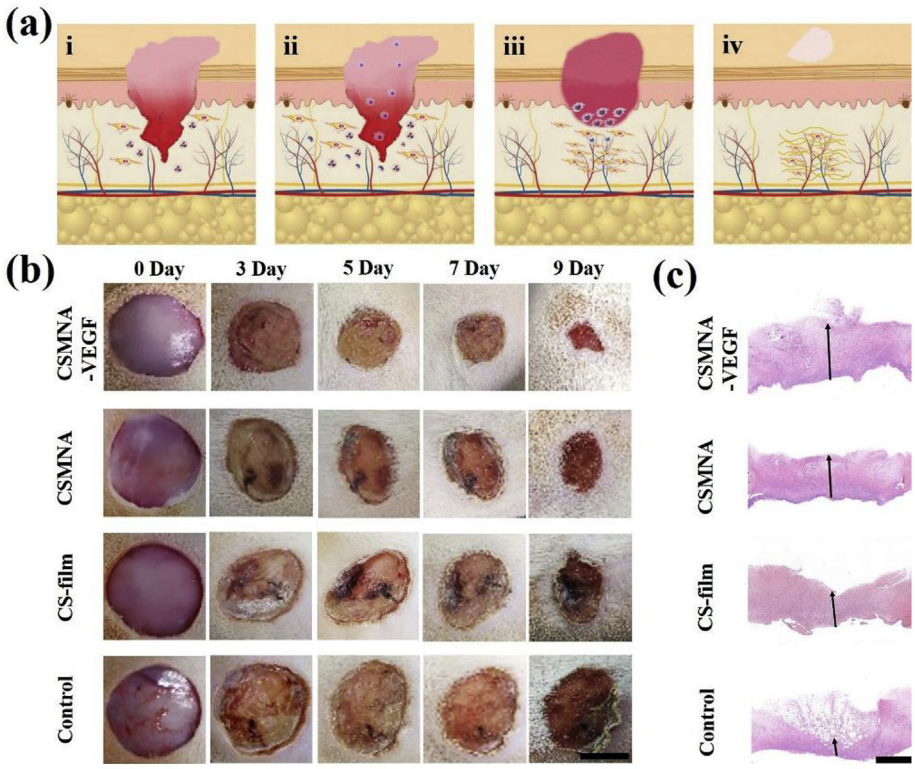

Fig. 4. Wound closure and H&E staining: (a) scheme of wound healing process: i) coagulation phase, ii) inflammation phase, iii) proliferation phase, (iv) remodeling phase; (b) images of the wounds treated with CSMNA-VEGF, CSMNA, CS-film and PBS solution (Control); (c) representative H&E staining of wounds after 9 days. Scale bars are 5 mm and 1 mm in (b) and (c), respectively.

inherent antibacterial property of CS could effectively protect the wound against bacterial infection. In addition, remodeling, marked as the last stage during wound healing, is usually reflected by the deposition of collagen as a skin component in the wound bed. Therefore, collagen deposition of all the groups was also evaluated. Results showed that the collagen deposited abundantly in the groups consisted of CS (Fig. 5c). Apparently, the CSMNA patch with VEGF achieved the greatest deposition of collagen, decreasing successively in group of CSMNA and plan CS film. And the control group performed with PBS solution presented the lowest deposition of collagen. The excellent anti-inflammatory effect and the remarkable collagen deposition indicated the potential application of CSMNA patch for wound-healing.

Except for the collagen deposition, angiogenesis is another necessary index during the remolding of tissue. Thus, to indicate neovascularization, double immunofluorescence staining of CD31, a marker of the vascular endothelial cell, and α-SMA, a marker of the vascular smooth muscle cells, were performed. Results showed that the density of vascular structure was obviously different in four groups (Fig. 6). For the control group, few positive results of CD31 and α-SMA immunostaining was observed, mainly attributed to the excess aggregation of immunocytes at the wound site responding to bacterial infection. Besides, the survival of normal cells, such like vascular endothelial

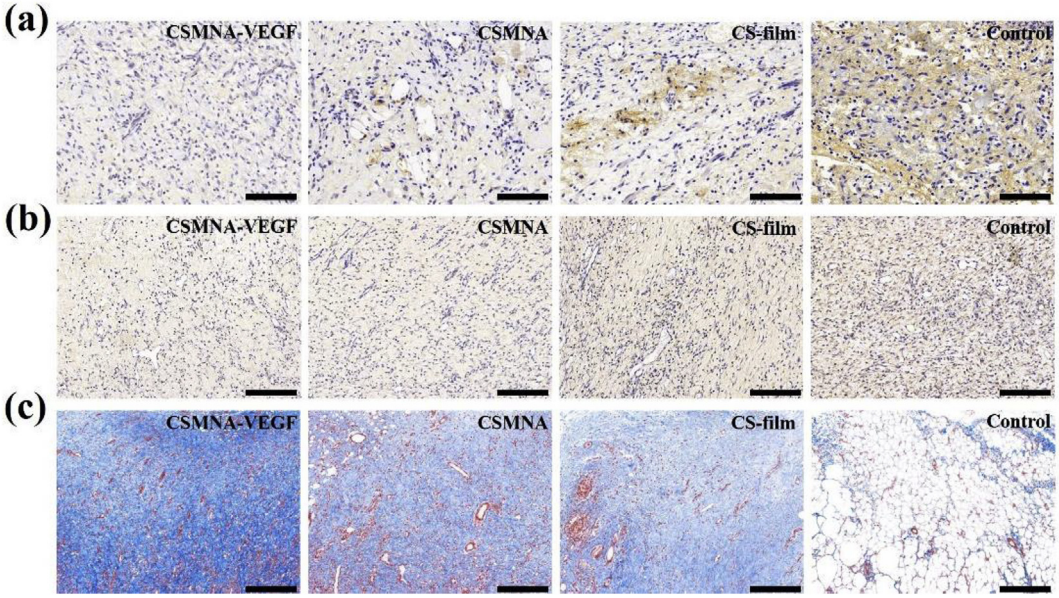

Fig. 5. Immunostaining of (a) IL-6 and (b) TNF-α of granulation tissues in different groups; (c) Masson's trichrome staining for collagen deposition after 9 days. Scale bars are 200 μm.

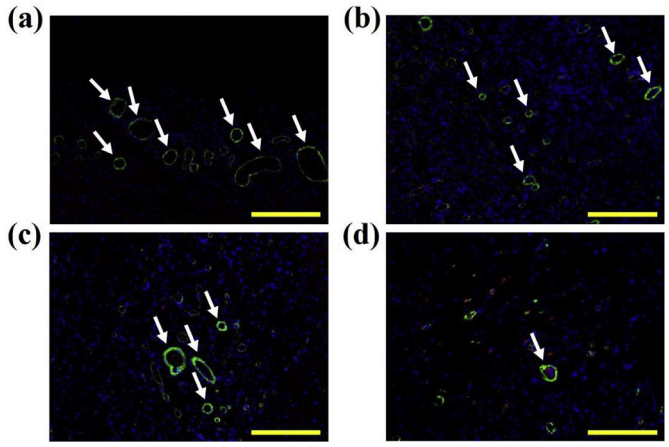

Fig. 6. Double immunofluorescence staining of neovascularization, $CD31^+$ structures (red) were surrounded by α-smooth muscle actin positive cells (green) (indicated with white arrows) in different group: (a) CSMNA-VEGF, (b) CSMNA, (c) CS-film, (d) Control. Scale bars are 50 μm.

cells and vascular smooth muscle cells was also negative, indicating few vascular structures in the wound site. Compared with the control group, the other groups presented a higher expression level of CD31 and α-SMA owing to the presence of CS, which could effectively reduce the bacterial infection induced inflammatory response. It is worth noting that the positive immunostaining areas of CD31 and α-SMA in the groups of CSMNA patch were more than the plane CS film group, indicating more vascular structures. Such differences between these groups could be attributed to the microstructure of the CSMNA, which possessed a non-planar surface morphology and larger specific surface and was beneficial to cells adhesion, migration and substance exchange. In addition, the maximum dense of vascular construction was found in CSMNA patch with VEGF group because the release of VEGF from the CSMNA could remarkably accelerate angiogenesis (Fig. S5, Supporting Information). This acceleration of angiogenesis in the reproductive tissue demonstrated the considerable capability of the CSMNA patch based drug delivery system in promoting wound healing.

4. Conclusion

In summary, we have developed and demonstrated a smart drug delivery system based on a form of versatile biomass hydrogel microneedle patch with controllable drug release capability for promoting wound healing. The microneedles were constituted by CS hydrogel, which possesses natural antibacterial property and has been widely utilized for wound healing. Owing to the microneedle structure, the CSMNA exhibited a superior capability of acceleration in inflammatory inhibition, collagen deposition, angiogenesis, and granulation tissue formation. Integrated with the temperature-responsive pNIPAM hydrogel, large doses of VEGF could be encapsulated in the pores of the CSMNA and controllably released into the wound sites, which dramatically promoted the wound healing in a severe infected wound model. These features indicate that the versatile biomass microneedle patch possesses great potential for promoting wound healing in practical applications.

CRediT authorship contribution statement

Junjie Chi: Formal analysis, Writing - original draft. **Xiaoxuan Zhang:** Writing - original draft. **Canwen Chen:** Formal analysis. **Changmin Shao:** Writing - original draft. **Yuanjin Zhao:** Writing - original draft. **Yongan Wang:** Writing - original draft.

Declaration of competing interest

The authors declare that they have no known competing financial interests or personal relationships that could have appeared to influence the work reported in this paper.

Acknowledgment

This work was supported by the National Natural Science Foundation of China (grants 61927805 and 51522302), the NSAF Foundation of China (grant U1530260), the Natural Science Foundation of Jiangsu (Grant no. BE2018707), the Special Fund for Military Medical Science (grants BWS16J007 and AWS17J009), and the China Postdoctoral Science Foundation funded project (2019M663090).

Appendix A. Supplementary data

Supplementary data to this article can be found online at https://doi.org/10.1016/j.bioactmat.2020.02.004.

References

[1] R. Xu, G. Luo, H. Xia, W. He, J. Zhao, B. Liu, J. Tan, J. Zhou, D. Liu, Y. Wang, Z. Yao, R. Zhan, S. Yang, J. Wu, Novel bilayer wound dressing composed of silicone rubber with particular micropores enhanced wound re-epithelialization and contraction, Biomaterials 40 (2015) 1–11.
[2] C. Gong, Q. Wu, Y. Wang, D. Zhang, F. Luo, X. Zhao, Y. Wei, Z. Qian, A biodegradable hydrogel system containing curcumin encapsulated in micelles for cutaneous wound healing, Biomaterials 34 (27) (2013) 6377–6387.
[3] S. Rani, T. Ritter, The Exosome-A maturally secreted nanoparticle and its application to wound healing, Adv. Mater. 28 (27) (2016) 5542–5552.
[4] D.R. Griffin, W.M. Weaver, P.O. Scumpia, D.D. Carlo, T. Segura, Accelerated wound healing by injectable microporous gel scaffolds assembled from annealed building blocks, Nat. Mater. 14 (7) (2015) 737.
[5] D.W. Grainger, Wound healing: enzymatically crosslinked scaffolds, Nat. Mater. 14 (7) (2015) 662.
[6] D. Liu, H. Zhang, F. Fontana, H.A. Santos, Microfluidic-assisted fabrication of carriers for controlled drug delivery, Lab Chip 17 (11) (2017) 1856–1883.
[7] J. Li, R. Cha, K. Mou, X. Zhao, K. Long, H. Luo, F. Zhou, X. Jiang, Nanocellulose-based antibacterial materials, Adv. Healthcare Mater. 7 (20) (2018) 1800334.
[8] W. Lai, H. Shum, Hypromellose-graft-chitosan and its polyelectrolyte complex as novel systems for sustained drug delivery, ACS Appl. Mater. Interfaces 7 (19) (2015) 10501–10510.
[9] Y. Liu, X. Zhao, C. Zhao, H. Zhang, Y. Zhao, Responsive porous microcarriers with controllable oxygen delivery for wound healing, Small 15 (21) (2019) 1901254.
[10] X. Sun, Q. Lang, H. Zhang, L. Cheng, Y. Zhang, G. Pang, X. Zhao, H. Yang, Y. Zhang, H.A. Santos, W. Cui, Electrospun photocrosslinkable hydrogel fibrous scaffolds for rapid in vivo vascularized skin flap regeneration, Adv. Funct. Mater. 27 (2) (2017) 1604617.
[11] P. Zhang, S. Wang, Designing fractal nanostructured biointerfaces for biomedical applications, ChemPhysChem 15 (8) (2014) 1550–1561.
[12] Y. Yu, G. Chen, J. Guo, Y. Liu, J. Ren, T. Kong, Y. Zhao, Vitamin metal-organic framework-laden microfibers from microfluidics for wound healing, Mater. Horiz. 5 (6) (2018) 1137–1142.
[13] L. Wu, Y. Gu, L. Liu, J. Tang, J. Mao, K. Xi, Z. Jiang, Y. Zhou, Y. Xu, L. Deng, L. Chen, W. Cui, Hierarchical micro/nanofibrous membranes of sustained releasing VEGF for periosteal regeneration, Biomaterials 227 (2019) 119555.
[14] C. Chen, Y. Liu, H. Wang, G. Chen, X. Wu, J. Ren, H. Zhang, Y. Zhao, Multifunctional chitosan inverse opal particles for wound healing, ACS Nano 12 (10) (2018) 10493–10500.
[15] L. Zhang, H. Bei, Y. Piao, Y. Wang, M. Yang, X. Zhao, Polymer-brush-grafted mesoporous silica nanoparticles for triggered drug delivery, ChemPhysChem 19 (16) (2018) 1956–1964.
[16] C. Chen, Y. Liu, L. Sun, G. Chen, X. Wu, J. Ren, Y. Zhao, Antibacterial porous microcarriers with a pathological state responsive switch for wound healing, ACS Appl. Bio Mater. 2 (5) (2019) 2155–2161.
[17] K. Lin, D. Zhang, M.H. Macedo, W. Cui, B. Sarmento, G. Shen, Advanced collagen-based biomaterials for regenerative biomedicine, Adv. Funct. Mater. 29 (3) (2019) 1804943.
[18] G. Chen, Y. Yu, G. Wang, G. Gu, X. Wu, J. Ren, H. Zhang, Y. Zhao, Microfluidic Electrospray Niacin Metal-Organic Frameworks Encapsulated Microcapsules for Wound Healing, Research, (2019) 61753982019.
[19] H. Chen, R. Cheng, X. Zhao, Y. Zhang, A. Tam, Y. Yan, H. Shen, Y.S. Zhang, J. Qi, Y. Feng, L. Liu, G. Pan, W. Cui, L. Deng, An injectable self-healing coordinative hydrogel with antibacterial and angiogenic properties for diabetic skin wound repair, NPG Asia Mater. 11 (1) (2019) 3.
[20] Z. Liu, Y. Li, W. Li, M. Kemell, S. Hietala, P. Figueiredo, L. Li, E. Mäkilä, M. Ma, J. Salonen, J.T. Hirvonen, D. Liu, H. Zhang, X. Deng, H.A. Santos, Close-loop dynamic nanohybrids on collagen-ark with in situ gelling transformation capability

for biomimetic stage-specific diabetic wound healing, Mater. Horiz. 6 (2) (2019) 385–393.
[21] J. Deng, Y. Tang, Q. Zhang, C. Wang, M. Liao, P. Ji, J. Song, G. Luo, L. Chen, X. Ran, Z. Wei, L. Zheng, R. Dang, X. Liu, H. Zhang, Y.S. Zhang, X. Zhang, H. Tan, A bioinspired medical adhesive derived from skin secretion of andrias davidianus for wound healing, Adv. Funct. Mater. 29 (2019) 1809110.
[22] W. Cui, L. Cheng, H. Li, Y. Zhou, Y. Zhang, J. Chang, Preparation of hydrophilic poly (L-lactide) electrospun fibrous scaffolds modified with chitosan for enhanced cell biocompatibility, Polymers 53 (11) (2012) 2298–2305.
[23] A. Mohandas, S. Deepthi, R. Biswas, R. Jayakumar, Chitosan based metallic nanocomposite scaffolds as antimicrobial wound dressings, Bioact. Mater. 3 (3) (2018) 267–277.
[24] Y. Liu, B. Workalemahu, X. Jiang, The effects of physicochemical properties of nanomaterials on their cellular uptake in vitro and in vivo, Small 13 (43) (2017) 1701815.
[25] M. Leonida, P. Ispas-Szabo, M.A. Mateescu, Self-stabilized chitosan and its complexes with carboxymethyl starch as excipients in drug delivery, Bioact. Mater 3 (3) (2018) 334–340.
[26] C. Berce, M.S. Muresan, O. Soritau, B. Petrushev, L. Tefas, I. Rigo, G. Ungureanu, C. Catoi, A. Irimie, C. Tomuleasa, Cutaneous wound healing using polymeric surgical dressings based on chitosan, sodium hyaluronate and resveratrol, A preclinical experimental study, Colloids Surf., B 163 (2018) 155–166.
[27] X. Zhang, G. Chen, F. Bian, L. Cai, Y. Zhao, Encoded microneedle arrays for detection of skin interstitial fluid biomarkers, Adv. Mater. 31 (37) (2019) 1902825.
[28] G. Yang, Q. Chen, D. Wen, Z. Chen, J. Wang, G. Chen, Z. Wang, X. Zhang, Y. Zhang, Q. Hu, L. Zhang, Z. Gu, A Therapeutic microneedle patch made from hair-derived keratin for promoting hair regrowth, ACS Nano 13 (4) (2019) 4354–4360.
[29] X. Zhang, Y. Yu, G. Chen, L. Sun, Y. Zhao, Biomimetic intestinal barrier based on microfluidic encapsulated sucralfate microcapsules, Sci. Bull. 64 (19) (2019) 1418–1425.
[30] G. Chen, J. Yu, Z. Gu, Glucose-responsive microneedle patches for diabetes treatment, J. Diabetes Sci. Technol. 13 (1) (2019) 41–48.
[31] H. Liu, S. Wang, Poly (N-isopropylacrylamide)-based thermo-responsive surfaces with controllable cell adhesion, Sci. China Chem. 57 (4) (2014) 552–557.
[32] C. Shao, Y. Liu, J. Chi, Z. Chen, J. Wang, Y. Zhao, Droplet microarray on patterned butterfly wing surfaces for cell spheroid culture, Langmuir 35 (10) (2019) 3832–3839.
[33] D. Shan, E. Gerhard, C. Zhang, J.W. Tierney, D. Xie, Z. Liu, J. Yang, Polymeric biomaterials for biophotonic applications, Bioact. Mater. 3 (4) (2018) 434–445.